GRIFFITH UNIVERSITY

Nonsequential double ionization of Ar in near-single-cycle laser pulses

Author

Chen, Zhangjin, Liu, Fang, Wen, Hua, Morishita, Toru, Zatsarinny, Oleg, Bartschat, Klaus

Published

2020

Journal Title

Optics Express

Version

Version of Record (VoR)

DOI

10.1364/OE.398035

Downloaded from

http://hdl.handle.net/10072/398797

Griffith Research Online

https://research-repository.griffith.edu.au

Research Article | Vol. 28, No. 15 / 20 July 2020 / Optics Express 22231
Optics EXPRESS

Nonsequential double ionization of Ar in near-single-cycle laser pulses

ZHANGJIN CHEN,[1,*] FANG LIU,[1] HUA WEN,[1] TORU MORISHITA,[2] OLEG ZATSARINNY,[3] AND KLAUS BARTSCHAT[3]

[1]Department of Physics, College of Science, Shantou University, Shantou, Guangdong 515063, China
[2]Institute for Advanced Science, The University of Electro-Communications, 1-5-1 Chofu-ga-oka, Chofu-shi, Tokyo 182-8585, Japan
[3]Department of Physics and Astronomy, Drake University, Des Moines, Iowa 50311, USA
[*]chenzj@stu.edu.cn

Abstract: Using the improved quantitative rescattering (QRS) model, we simulate the correlated two-electron momentum distributions (CMD) for nonsequential double ionization (NSDI) of Ar by near-single-cycle laser pulses with a wavelength of 750 nm at an intensity of 2.8×10^{14} W/cm^2. With the accurate cross sections obtained from fully quantum mechanical calculations for both electron impact excitation and electron impact ionization of Ar^+, we unambiguously identify the contributions from recollision direct ionization (RDI) and recollision excitation with subsequent ionization (RESI). Our analysis reveals that RESI constitutes the main contribution to NSDI of Ar under the conditions considered here. The simulated results are directly compared with experimental measurements [Bergues *et al.*, Nature Commun. **3**, 813 (2012)] in which each NSDI event is tagged with the carrier-envelope phase (CEP). It is found that the overall pattern of both the CEP-resolved and the CEP-averaged CMDs measured in experiment are well reproduced by the QRS model, and the cross-shaped structure in the CEP-averaged CMD is attributed to the strong forward scattering of the recolliding electron as well as the depletion effect in tunneling ionization of the electron from an excited state of the parent ion.

© 2020 Optical Society of America under the terms of the OSA Open Access Publishing Agreement

1. Introduction

Over the past three decades, nonsequential double ionization (NSDI) has been the subject of numerous experimental and theoretical studies (for a review, see [1]). The principal underlying physical mechanisms leading to NSDI were initially revealed by the prominent "knee" structure observed in pioneering experiments, in which the yield of doubly charged ions was measured as a function of the laser intensity [2,3]. However, since many characteristic structures of that particular process are smoothed out in the total yield of doubly charged ions, these measurements could only give limited insight into the dynamics of laser-electron and electron-electron interaction in NSDI. In contrast, the correlated two-electron momentum distributions (CMDs) provide much more detailed information on NSDI. The first kinematically complete experiments were performed, at the turn of this century, by Weber *et al.* who measured the CMD of NSDI for Ar [4]. It was found that, generally, electrons are more likely to be emitted nearly parallel to each other, such that the first and third quadrants of the CMD accommodate more electrons [4–7]. On the other hand, when the laser intensity is close to or even slightly below threshold, so-called "anti-correlation" has also been observed, where back-to-back emission dominates and hence the two released electrons concentrate in the second and fourth quadrants [8].

The coincident electron momentum distributions shed more light on the mechanisms responsible for NSDI, and they have attracted utmost attention by theorists. It is now widely accepted that the correlated character of the electron emission in NSDI is a consequence of the rescattering process [9,10]. In the rescattering picture, a first electron, liberated via tunnel ionization, is accelerated by the laser field and driven back to the parent ion. Then the laser-induced electron

#398035 https://doi.org/10.1364/OE.398035
Journal © 2020 Received 19 May 2020; revised 24 Jun 2020; accepted 30 Jun 2020; published 13 Jul 2020

Optics EXPRESS

may recollide with the parent ion, leading to a second electron being ionized through recollision direct ionization (RDI) or recollision excitation with subsequent ionization (RESI). However, in conventional experiments using multi-cycle laser pulses, multiple recollisions of the first electron with the parent ion may significantly complicate the NSDI dynamics, thereby impeding the understanding of the exact mechanisms responsible for the observed energy and momentum sharing between the electrons generated in the process. In this sense, the ideal condition for experiment is to confine NSDI to a single-cycle laser pulse.

The first CMD measurement for NSDI in the near-single-cycle limit was carried out by Bergues *et al.* [11] who used carrier-envelope phase (CEP)-tagged near-single-cycle pulses, in which the cross-shaped structure observed in the CEP-averaged CMD qualitatively differs from those recorded in all previous experiments using many-cycle pulses. As a new milestone in the experimental research of NSDI, such measurements yield direct and intuitive insight into the dynamics, since the kinematically complete single-cycle NSDI experiments require a reduced level of complexity for modeling.

The experimental findings of Bergues *et al.* [11] have been explored by a few theoretical studies [11–15]. Together with the experimental data, Bergues *et al.* [11] also presented theoretical simulations using a simple one-dimensional (1D) semiclassical model. By taking into account only the lowest excited state of Ar^+ and assuming a scattering angle $\beta = 20^\circ$ in RESI, the semiclassical model reproduced the cross-shaped structure and ascribed the asymmetric energy sharing to a depletion effect. In contrast, without resorting to depletion, the *S*-matrix calculations revealed that the cross shape results from the excitation from a $3p$ to a $4s$ state [12]. However, further experimental investigations demonstrated that the measured NSDI spectra of N_2 and Ar exposed to near-single-cycle laser pulses exhibit a striking resemblance [16], which implies that the cross shape is not the result of the excitation from a $3p$ to a $4s$ state. Interestingly, while the contribution of RDI is neglected in the 1D semiclassical simulations [11], *ab initio* calculations with a three-dimensional (3D) classical ensemble model indicate that the RDI significantly contributes to the cross-shaped structure [13]. It should be noted that, although the 1D semiclassical model captures the essential features of the data, electron correlations enter the model incompletely via the ionic excitation and the scattering angle [11,14]. On the other hand, in the 3D classical simulations of [13], two Coulomb softening parameters were introduced to prevent autoionization and avoid a numerical singularity. Recently, Chen *et al.* [15] studied the NSDI processes of Ar driven by a near-infrared near-single-cycle laser pulse by employing a 3D semiclassical model without using a free parameter. This 3D model, indeed, has an advantage over models that soften the Coulomb potential [13]. Similar to the analysis performed in [13], by tracing the classical trajectories of NSDI, Chen *et al.* [15] also found that both RDI and RESI significantly contribute. Nevertheless, comparisons of the model results with the observed data presented in [15] showed that, at least for the CEP-averaged CMD, significant discrepancies exist between theory and experiment.

Even though these classical calculations provide valuable insights into the mechanisms of NSDI processes in near-single-cycle laser pulses, the exact underlying physics still remains debatable. Therefore, it is desirable to employ a theoretical model in which the electron and the target atom are described using quantum mechanics.

The quantitative rescattering (QRS) model for NSDI developed one decade ago [17,18] is a full quantum theory based on the rescattering model. Recently, the QRS model was modified by taking into account the lowering of the threshold energy due to the presence of an electric field at the instant of recollision [19]. This improvement enables the QRS model to deal with NSDI at intensities below threshold. With the improved QRS model, we revisited both the RDI and RESI in NSDI of helium in 800-nm laser fields [20,21]. It was found that in the simulated CMD for RESI, the fourfold symmetry with regard to the parallel momentum components is broken

Optics EXPRESS

[21] and the final-state electron repulsion always plays an important role in RDI even at high intensities [22].

In the present paper, we use the improved QRS model [20,21] to study the correlated electron emission in NSDI of Ar by linearly polarized laser pulses with a wavelength of 750 nm and a pulse duration (FWHM) of 4 fs. Our aim is to identify the contributions of RDI and RESI and unveil the underlying mechanisms responsible for the observed cross-shaped structure from a quantum-mechanical point of view.

Atomic units (a.u.) are used in this paper unless otherwise specified.

2. Theoretical model

While laser-induced rescattering processes can be qualitatively interpreted by the classical rescattering model [9,10], the QRS model, based on the factorization formula in [23–26], provides a quantitative description. The past decade has witnessed great success of the QRS model in dealing with various laser-induced rescattering processes, including high-order above-threshold ionization (HATI) [23,27], high-order harmonic generation [23,28], and NSDI [29]. The only difference between all these laser-induced rescattering processes lies in the type of recollision between the returning electron and the parent ion. Before the recollision, they all share the same process, i.e., a tunnel-ionized electron is driven back to the parent ion by the laser field. In the QRS model, the momentum (energy) distribution of the laser-induced returning electron is described by a returning-electron wave packet (RWP) that is expressed as [27]

$$W(k_r) = D(p,\theta)/\frac{\mathrm{d}\sigma^{\mathrm{el}}(k_r,\theta_r)}{\mathrm{d}\Omega_r}, \tag{1}$$

where $D(p,\theta)$ is the momentum distribution of HATI photoelectrons, due to elastic scattering of the returning electron from the parent ion, with momentum of magnitude p at a detection angle θ with respect to the polarization of the laser field, and $\mathrm{d}\sigma^{\mathrm{el}}(k_r,\theta_r)/\mathrm{d}\Omega_r$ is the differential cross section (DCS) for laser-free e-Ar^+ elastic scattering with a momentum of magnitude k_r at an angle θ_r with respect to the direction of the returning electron. The detected photoelectron momentum $\mathbf{p}$ and the momentum $\mathbf{k}_r$ of the scattered electron are related by

$$\mathbf{p} = \mathbf{k}_r - \mathbf{A}_r, \tag{2}$$

where $\mathbf{A}_r$ is the instantaneous vector potential at the time of recollision. For high-energy returning electrons that are important for NSDI processes, we use the relation [27]

$$k_r = 1.26|A_r|. \tag{3}$$

In Eq. (1), the elastic scattering DCS is calculated within the plane-wave first Born approximation, and the momentum distribution $D(p,\theta)$ for high-energy photoelectrons is evaluated based on the improved strong-field approximation (SFA) for HATI [27]. We note that an analytical expression of the RWP for HATI at the outermost backward rescattering caustic was recently derived based on the adiabatic theory for azimuthal quantum number $m = 0$ [24] and for arbitrary m [26].

According to the QRS model, the CMD of RESI for the momentum components $p_1^{||}$ and $p_2^{||}$ of the two outgoing electrons along the laser polarization direction is expressed by

$$D_{E_i}^{\mathrm{RESI}}(p_1^{||},p_2^{||}) = D_{E_i}^{\mathrm{exc}}(p_1^{||}) \times D^{\mathrm{tun}}(p_2^{||}) \tag{4}$$

where $D_{E_i}^{\mathrm{exc}}(p_1^{||})$ and $D^{\mathrm{tun}}(p_2^{||})$ are the parallel momentum distributions for the returning electron with kinetic energy E_i after recollision and the electron tunneling-ionized from an excited state of the parent ion, respectively.

Optics EXPRESS

The parallel momentum distribution $D_{E_i}^{\rm exc}(p_1^{||})$ is obtained by projecting the DCS for electron impact excitation of Ar^+ onto the polarization direction to which the parallel momentum $k_1^{||}$ of the projectile electron is shifted by $-A_r$ [21], i.e.,

$$p_1^{||} = k_1^{||} - A_r. \tag{5}$$

The DCS for electron impact excitation of Ar^+ is calculated by using the state-of-the-art multi-electron B-spline R-matrix (BSR) close-coupling theory [30,31]. The parallel momentum distribution $D^{\rm tun}(p_2^{||})$ for tunneling ionization of an electron from an excited state is calculated by integrating the two-dimensional (2D) momentum distribution for single ionization over the momentum component perpendicular to the laser polarization. Here, the 2D momentum distribution for single ionization of Ar^+ is evaluated by solving the time dependent Schrödinger equation (TDSE) [21,32].

Equation (4) only represents the CMD for RESI at a fixed incident (returning) electron energy. For a given intensity, in principle, excitation can occur as long as the kinetic energy of the returning electron is larger than the lowered threshold excitation energy. Therefore, the contributions from collisions at all incident energies should be considered. Consequently, in Eq. (4), an integral over E_i should be performed. This gives

$$D_{\rm RESI}(p_1^{||}, p_2^{||}) = \int_{I_p^{\rm exc}}^{\infty} {\rm d}E_i \, D_{E_i}^{\rm RESI}(p_1^{||}, p_2^{||}) \, W(E_i - \Delta E_{\rm exc}), \tag{6}$$

where $I_p^{\rm exc}$ is the threshold energy for excitation, $W(E)$ is the RWP with energy $E = k_r^2/2$, and $\Delta E_{\rm exc}$ is the downward shift of the threshold excitation energy due to the presence of an electric field F_r at the instant of recollision. The latter is given by [33]

$$\Delta E_{\rm exc} = 2\sqrt{|F_r|}. \tag{7}$$

The method used to determine F_r was presented in [20].

Similarly, the CMD for RDI can be obtained by projecting the triple-differential cross section (TDCS) for electron impact ionization of the parent ion onto the polarization direction and shifting the parallel momenta of the two outgoing electrons by $-A_r$:

$$D_{\rm RDI}(p_1^{||}, p_2^{||}) = \int_{I_p^{e2e}}^{\infty} {\rm d}E_i \, D_{E_i}^{\rm RDI}(p_1^{||}, p_2^{||}) \, W(E_i - \Delta E_{e2e}). \tag{8}$$

Here I_p^{e2e} is the threshold energy for ionization, $D_{E_i}^{\rm RDI}(p_1^{||}, p_2^{||})$ is the CMD for the laser-induced recollision $(e, 2e)$ process at incident energy E_i, and ΔE_{e2e} is the downward shift of the threshold ionization energy given by [34]

$$\Delta E_{e2e} = 2\sqrt{2|F_r|}. \tag{9}$$

The TDCS for laser-free $(e, 2e)$ on Ar^+ is calculated based on the distorted-wave Born approximation (DWBA) [35,36]. Standard partial-wave expansions are made to evaluate the scattering amplitude.

Correspondingly, to account for the lower threshold, Eq. (3) should be modified and rewritten as

$$|A_r| = \sqrt{2(E_i - \Delta E_j)}/1.26, \tag{10}$$

where j stands for "exc" or "$e2e$".

Details of the numerical procedures for simulations of the CMD for NSDI of atoms based on the improved QRS model were presented in [20,21,37].

Optics EXPRESS

3. Results and discussion

We aim to simulate the CMD for NSDI of Ar in 4 fs linearly polarized laser pulses at 750 nm [11]. The laser intensity used in the experiment was given as $(3.0 \pm 0.6) \times 10^{14}$ W/cm^2. According to the rescattering model, the highest energy of the laser-induced returning electron is $3.17U_p$, where U_p is the ponderomotive energy. Therefore, under the experimental conditions considered here, the maximum collision energy is around 50 eV, which indicates that both RESI and RDI contribute to NSDI of Ar.

3.1. Correlated momentum distributions for RESI

We first simulate the CMD for RESI in NSDI of Ar. In the QRS model, the momentum distributions for the two outgoing electrons in RESI are simulated separately.

To obtain the parallel momentum distributions $D_{E_i}^{\rm exc}(p_1^{||})$ in Eq. (4) for the returning electron after recollision, we need to prepare the DCS for laser-free electron impact excitation of Ar^+. In Figs. 1(a)–1(c), we plot the DCSs, obtained with the BSR code, for electron impact excitation of Ar^+ from the ground state to the excited states of $3d$, $4s$, and $4p$ at incident energies of 20, 30, 40 and 50 eV, respectively. As expected, as the incident energy increases, forward scattering becomes dominant. The complex structures in the angular dependence of the DCS at large angles have little effect on the angle-integrated cross section. Figure 1(d) shows the TCSs for electron impact excitation of Ar^+ to the excited states of $3s3p^6$, $3d$, $4s$, and $4p$. It can be seen from Fig. 1(d) that excitation to $3d$ dominates due to the large overlap of the $3p$ and $3d$ orbitals. On the other hand, the TCS for excitation to the lowest excited state $3s3p^6$ is more than ten times smaller than that for $3d$ at collision energies higher than 20 eV. This is due to the fact that at high energies, cross sections are proportional to the corresponding oscillator strengths. The f-value for the $3p^5$-$3s3p^6$ transition is 0.01 (surprisingly small), whereas the sum of the f-values for transitions to the $3p^43d$ levels is 5.4. Figure 1(d) also displays the TCS for electron impact ionization of Ar^+ calculated by using the semiempirical formula of Lotz [38], which turned out to be in very good agreement with the experimental findings [39]. The TCS for $(e, 2e)$ demonstrates that RDI does contribute to NSDI, but the contribution is not significant compared to that of RESI, since both RDI and RESI share the same RWP. Since the DWBA model does not reproduce the correct absolute TCS, the TDCS obtained from the DWBA model at each incident energy were renormalized according to the TCS from Lotz formula.

By projecting the calculated DCSs for electron impact excitation of Ar^+ onto the polarization direction with the parallel momentum shifted by $-A_r$, we obtain the parallel momentum distributions for the returning electron after recollision in NSDI of Ar by 750 nm and 4 fs laser pulses at an intensity of 2.8×10^{14} W/cm^2. In the present work, the linearly polarized electric field $\mathbf{F}(t)$ of the laser pulse along the z axis is given by

$$\mathbf{F}(t) = F_0 \cos^2\left(\frac{\pi t}{\tau}\right) \cos(\omega t + \phi)\hat{z} \tag{11}$$

for the time interval $(-\tau/2, \tau/2)$ and zero elsewhere. Here τ is the full duration of the laser pulse, which is 2.75 times of the FWHM, ω is the carrier frequency, and ϕ is the CEP.

In Figs. 2(a)–2(c), we plot the parallel momentum distributions for the returning electron after recolliding with the Ar^+ ion and exciting the residual ground-state electron to the excited states of $3d$, $4s$, and $4p$ at energies of 20, 30, 40, and 50 eV, respectively. The results shown in Figs. 2(a)–2(c) are for the situation in which the CEP of the laser field is 65° and the laser-induced electron returns to the parent ion along the $-\hat{z}$-direction. For this situation, the smallest and largest parallel momenta correspond to rescattering angles of $\theta_r = 0°$ and 180°, respectively. As expected, the momentum distributions exhibit a very similar behavior as those of the DCSs.

Figures 2(d)–2(f) exhibit the parallel momentum distributions evaluated by solving the TDSE for electrons tunneling-ionized from the excited $3d$, $4s$, and $4p$ states, respectively. The main

Optics EXPRESS

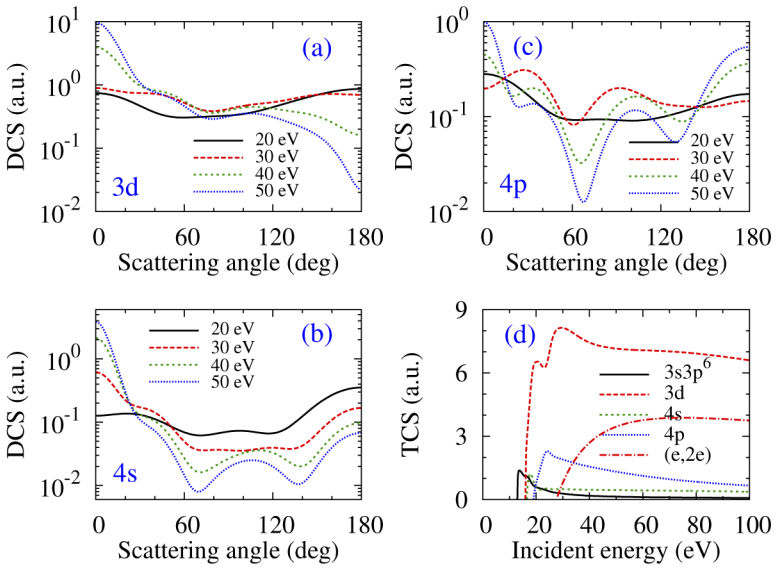

Fig. 1. Differential cross section for electron impact excitation of Ar^+ from the ground state to the excited states $3d$ (a), $4s$ (b), and $4p$ (c) at incident energies of 20, 30, 40, and 50 eV, respectively. In panel (d), the total cross sections for electron impact excitation of Ar^+ to the excited states of $3s3p^6$, $3d$, $4s$, and $4p$ and electron impact ionization of Ar^+ from the ground state are also displayed. For excitation, all results were obtained with the BSR code. For ionization, the total cross sections were calculated by using the semiempirical formula of Lotz.

characteristic feature of these distributions is their asymmetry. With respect to $p_2^{||} = 0$, (i) the "right" and "left" distributions are not symmetric, (ii) each of the momentum distributions is not symmetric either, and (iii) the asymmetry is more pronounced for higher excited states. As will be explained below, the notations "right" and "left" used here refer to the situations in which the laser-induced electron returns to the parent ion along $-\hat{z}$ and $+\hat{z}$, respectively.

While the TDSE calculations do not provide much insight into the underlying physics, the principal physics of tunneling ionization can be directly unveiled by the Ammosov-Delone-Krainov (ADK) model [40]. For a better understanding, therefore, we show how to obtain the parallel momentum distributions for the tunneling-ionized electron from the ADK rate. With the depletion effect taken into account, the ionization rate can be expressed as

$$Y^{\mathrm{ADK}}(t) = W\left[|F(t)|\right] e^{-\int_{t_0}^{t} W[|F(t')|]dt'}, \tag{12}$$

where $W\left[|F(t)|\right]$ is the modified ADK rate given by Eq. (2) in [41], and t_0 is the time at which tunneling ionization begins. It should be noted that the exponential term in Eq. (12) accounts for depletion.

Figure 3(a) displays the ionization rate of Ar^+ from $3d$ ($m = 0$) in a 750 nm, 4 fs laser pulse at an intensity of 2.8×10^{14} W/cm^2 with a CEP of 65°. The solid black (broken red) curve shows the ionization rate for tunneling that begins at recollision time t_3 (t_4) when the vector potential is negative (positive), corresponding to the ionization time around t_1 (t_2) of the first electron that returns to the parent ion along the $-\hat{z}$ ($+\hat{z}$) direction. It can be seen that ionization starting at an earlier time t_3 continues for a longer time (more than half a cycle) with a larger ionization rate compared to that begins at t_4. In addition, due to the depletion effect, the ADK rates are not symmetric with respect to the local field maxima.

Optics EXPRESS

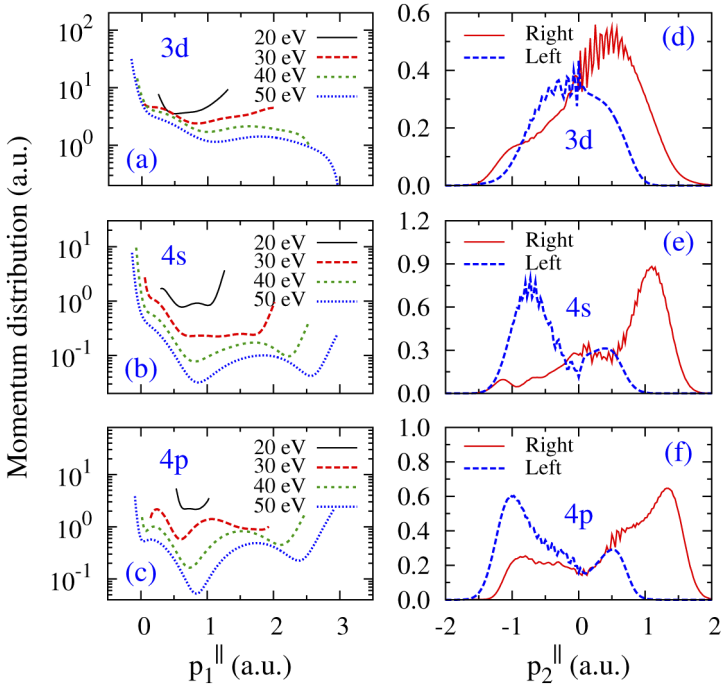

Fig. 2. Parallel momentum distributions for two outgoing electrons in NSDI of Ar by a 750 nm, 4 fs laser pulse at an intensity of 2.8×10^{14} W/cm^2 with a CEP of 65°. Results are shown for the active electron after recolliding with the Ar^+ ion and exciting the residual ground-state electron to the excited states $3d$ (a), $4s$ (b), and $4p$ (c) at energies of 20, 30, 40, and 50 eV for the situation in which the laser-induced electron returns to the parent ion along the $-\hat{z}$ direction, and for the tunneling electron ionized from Ar^+ in the excited states $3d$ (d), $4s$ (e), and $4p$ (f).

From the ionization rate, the parallel momentum distribution can be evaluated by

$$D^{\mathrm{ADK}}(p_2^{||}) = D^{\mathrm{ADK}}[-A(t)] = \frac{1}{|E(t)|} Y^{\mathrm{ADK}}(t). \tag{13}$$

In Figs. 3(b) and 3(c), we show the parallel momentum distributions obtained from the ADK rates displayed in Fig. 3(a) and compare them with the corresponding ones from TDSE. In the TDSE calculations for ionization of electron from an excited state of Ar^+, only the part of laser pulse after recollision time is used. Explicitly, as shown in Fig. 3(a), for $\phi = 65°$, the part of electric field starting from t_3 (t_4) to the end of pulse is used in the TDSE calculations for the "right" ("left") parallel momentum distributions of tunneling-ionized electron. As indicated in Fig. 3, here we use the labels "right" ("left") for the situation in which the vector potential is negative (positive) at the instant of recollision. This is due to the fact that, in the 2D momentum spectra of HATI, the right (left) side with p_z>0 (p_z<0) accommodates high-energy photoelectrons resulting from elastic scattering of the returning electron with the parent ion taking place at the instant when the vector potential is negative (positive) [27]. While the range of the momentum distribution obtained from the ADK model is within $[-A_0, A_0]$, where $A_0 = 1.47$ is the maximum value of the vector potential for the case considered here, wider momentum distributions are predicted when solving the TDSE. Nevertheless, similar to those obtained by solving the TDSE, the momentum distributions of ADK are also asymmetric with respect to $p_2^{||} = 0$. It can be seen from Fig. 3(a) that the asymmetry is due to depletion of the excited Ar^+ population. Furthermore,

Optics EXPRESS

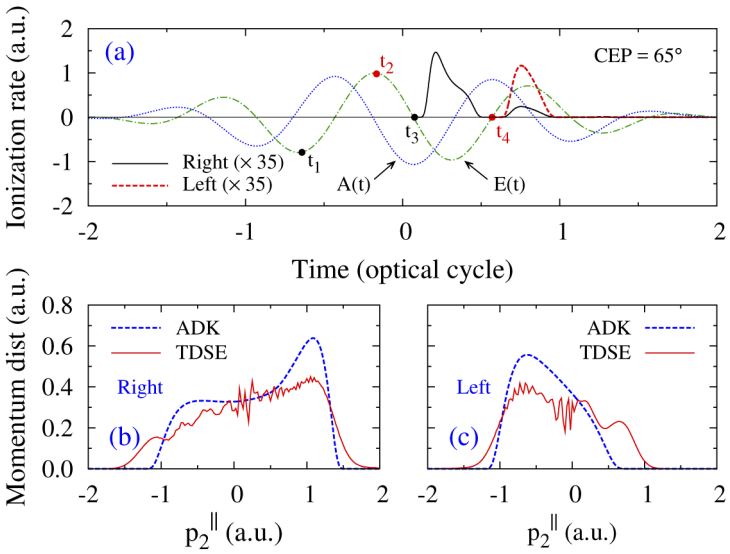

Fig. 3. (a) ADK rate for ionization of Ar^+ from $3d$ ($m = 0$) in a 750 nm, 4 fs laser pulse at an intensity of 2.8×10^{14} W/cm^2 with a CEP of 65°. The electric field (green chain curve) and the vector potential (blue dotted curve) of the laser field, both normalized to unity, are also indicated. (b) Comparison of parallel momentum distributions corresponding to the ADK rate with the TDSE results for the situation in which the laser-induced electron returns to the parent ion along the $-\hat{z}$ direction. (c) Same as (b), except that the laser-induced electron returns to the parent ion along the $+\hat{z}$ direction.

by integrating the momentum distributions over $p_2^{||}$, we found that the total ionization yields for right and left sides are not the same. This is quite different from the situation in which a flat top envelope is used in the simulations for long pulses [21,42].

Another ingredient to be evaluated in Eq. (6) is the RWP. Again, different from the situation for long pulses in which the right and left RWPs are almost the same, for short pulses the right- and left-side RWPs need to be calculated separately for each CEP. Figure 4 shows the right- and left-side RWPs for single ionization of Ar in 750 nm, 4 fs laser pulses at an intensity of 2.8×10^{14} W/cm^2 with CEPs of 5°, 35°, 65°, 95°, 125°, and 155°, respectively. For CEPs from 180° to 360°, the left and right sides are simply interchanged. Clearly, the RWP exhibits a strong dependence on the CEP, and the right-side RWP differs remarkably from the left-side one for all the CEPs considered here. Each RWP decreases dramatically at low energies with increasing energy, followed by a plateau in the high-energy region with some oscillations until a cut-off is reached. Generally, the left-side RWP becomes weaker and extends to higher energy as the CEP increases, while the trend reverses for the right-side RWP.

With the evaluated parallel momentum distributions for returning electron after recollision and the tunneling electron ionized from an excited state, respectively, the CMD for RESI at a given intensity and a fixed incident energy can be simulated by using Eq. (4). Figures 5(a) and 5(b) display the CMD for RESI of Ar in a 750 nm, 4 fs laser pulse at an intensity of 2.8×10^{14} W/cm^2 with $\phi = 65°$ for the situations in which the tunneling electron is ionized from $Ar^+(3d)$ and the laser-induced electron returns to the parent ion along the direction of $-\hat{z}$ with energies of 30 eV and 40 eV, respectively. In the CMD, the distribution along $p_1^{||}$ directly reflects the momentum distribution of the returning electron after recollision. The pattern of the momentum distribution along $p_1^{||}$ for a recollision energy of 30 eV in Fig. 5(a) differs significantly from that for 40 eV in Fig. 5(b). In Fig. 5(a), the dense populations along $p_1^{||}$ at both small and large

Optics EXPRESS

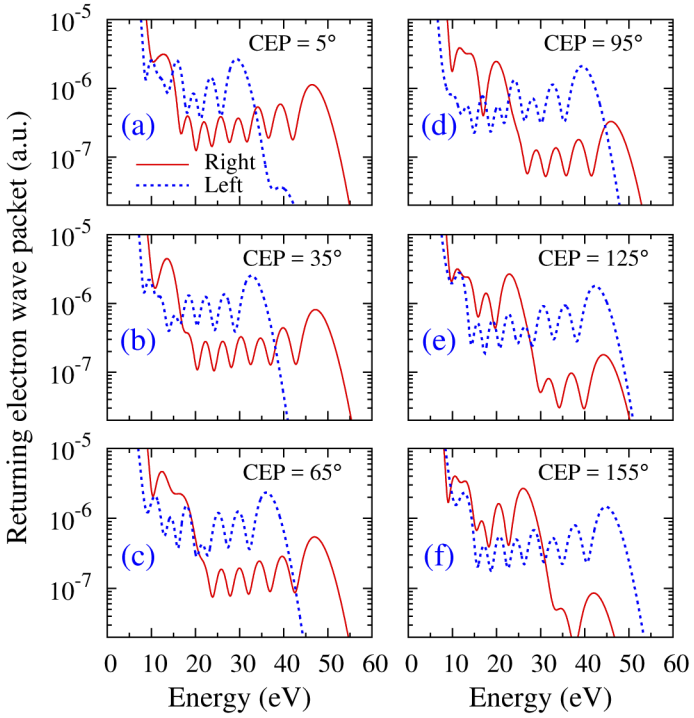

Fig. 4. Returning electron wave packets for single ionization of Ar in 750 nm, 4 fs laser pulses at an intensity of 2.8×10^{14} W/cm^2 with a CEP of 5° (a), 35° (b) 65° (c), 95° (d), 125° (e), and 155° (f).

momenta indicate that backward scattering is comparable to forward scattering. As demonstrated in Fig. 2(a), forward scattering becomes dominant as the incident energy increases to 40 eV. This explains why the CMD in Fig. 5(b) exhibits a sharp distribution at small $p_1^{||}$. On the other hand, the distribution along $p_2^{||}$ in the CMD represents the momentum distribution of the tunneling electron. As shown in Fig. 2(d), the right-side momentum distribution of the tunneling electron ionized from $Ar^+(3d)$ is asymmetric with respect to $p_2^{||} = 0$ with a peak locating around $p_2^{||} = 0.5$. As a result, the densest distribution along $p_2^{||}$ in Figs. 5(a) and 5(b) appears around $p_2^{||} = 0.5$. The CMDs shown in Figs. 5(d) and 5(e) can be understood in the same way as those in Figs. 5(a) and 5(b), except that the laser-induced electron returns to the parent ion along the $+\hat{z}$ direction. Hence most NSDI events appear in the region of $p_1^{||}<0$, but forward scattering also corresponds to the small absolute value of $p_1^{||}$.

Once the CMDs for all possible recollision energies have been calculated, the CMD for RESI at a given intensity can be obtained by summing up the CMDs for each individual energy weighted by the RWP, as expressed by Eq. (6). For the intensity of 2.8×10^{14} W/cm^2, the integrated CMDs are displayed in Figs. 5(c) and 5(f) for the right and left sides, respectively. The patterns of the right- and left-side CMD strongly depend on the RWP. As shown in Fig. 4(c), the right-side RWP extends to higher energies with a magnitude a few times smaller than the left-side one for energies above 20 eV. Since forward scattering is more pronounced at higher impact energy, in the right-side CMD the correlated electron pairs cluster in the region where the momentum of the returning electron after recollision is close to zero, while in the left-side CMD a considerable number of NSDI events distribute far away from $p_1^{||} = 0$. This clearly indicates that the RWP plays

Optics EXPRESS

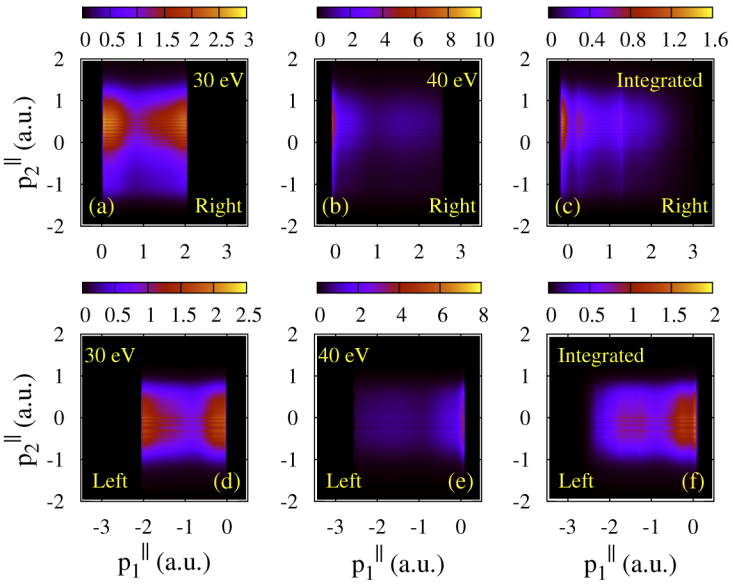

Fig. 5. Correlated two-electron parallel momentum distributions for excitation-tunneling in NSDI of Ar in a 750 nm, 4 fs laser pulse at an intensity of 2.8×10^{14} W/cm^2 with a CEP of 65° for the tunneling electron ionized from $Ar^+(3d)$: (a,d) Right and left sides for E_i = 30 eV; (b,e) right and left sides for E_i = 40 eV; (c,f) right and left sides for all incident energies.

an important role in predicting the structure of CMD when the contributions from recollisions at all possible incident energies are considered.

Due to the indistinguishability of the two outgoing electrons, the CMD for RESI should be symmetric with respect to the main diagonal $p_1^{||} = p_2^{||}$. By symmetrizing the CMD for both right and left sides, as displayed in Fig. 5, we obtain the full-space CMD for RESI. Figure 6 depicts the full-space CMD for RESI of Ar in 750 nm, 4 fs laser pulses at an intensity of 2.8×10^{14} W/cm^2 with six CEPs ranging from 5° to 155° in steps of 30°. [A movie showing the CEP dependence of the CMD in 3D space is also provided; see Visualization 1.] In Fig. 6, we have considered excitation-tunneling from the excited states 3*d*, 4*s* and 4*p* of Ar^+. As expected, and different from the case of long pulses, the CEP-resolved CMDs for short pulses are asymmetric with respect to the minor diagonal $p_1^{||} = -p_2^{||}$. Despite the strong dependence on the CEP, the CMDs for all the CEPs exhibit a similar pattern in that one of the two outgoing electrons always prefers to escape with a near-zero final momentum in the polarization direction, whereas the other one most likely drifts out with a significantly nonzero final longitudinal momentum. This is due to the strong forward scattering of the recolliding electron, as demonstrated in Fig. 5. This analysis is consistent with the conclusion drawn from the 1D semiclassical model employed by Bergues *et al.* in [11]. However, it should be noted that all scattering angles have been considered in the present simulations, while only one selected scattering angle was involved in the 1D semiclassical simulations [11]. In fact, to confine the final momentum of the recolliding electron to small values around zero, Bergues *et al.* [11] introduced a free parameter β that denotes the angle between the electron momentum just before and just after the recollision. They then set $\beta = 20°$, since neither the electron impact excitation cross sections nor the scattering angles were known.

Optics EXPRESS

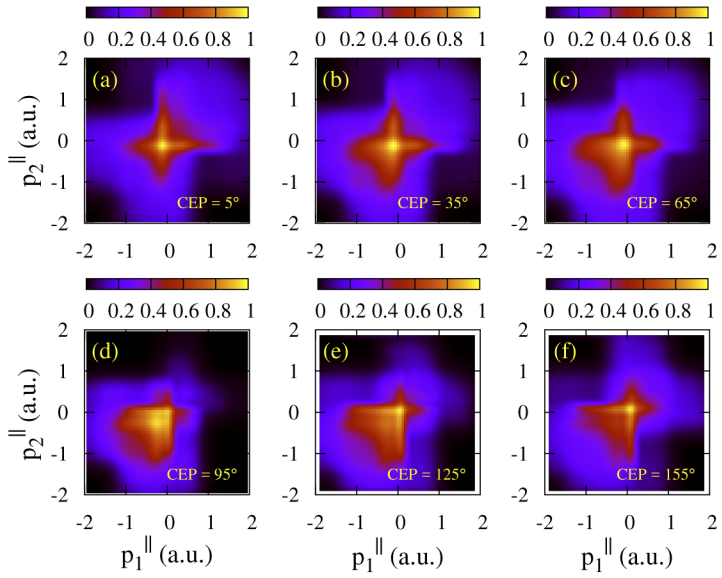

Fig. 6. Normalized correlated two-electron parallel momentum distributions for excitation-tunneling in NSDI of Ar in 750 nm, 4 fs laser pulses at an intensity of 2.8×10^{14} W/cm^2 with a CEP of 5° (a), 35° (b), 65° (c), 95° (d), 125° (e), and 155° (f).

3.2. Comparison with experiment including both RESI and RDI

3.2.1. Ar^{2+} asymmetry

The asymmetry of the CEP-resolved CMD with respect to $p_1^{||} = -p_2^{||}$ can be represented by the parameter $A = (N^+ - N^-)/(N^+ + N^-)$, where N^+ and N^- are the number of double ionization events above and below the minor diagonal, respectively. From the simulated CMD for RESI we obtain the Ar^{2+} asymmetry as a function of the CEP, which is compared with experiment in Fig. 7. By choosing an intensity of 2.8×10^{14} W/cm^2, the amplitude of the simulated asymmetry curve exactly matches the measured Ar^{2+} asymmetry, while the phase of the predicted Ar^{2+} asymmetry deviates from experiment by a shift of 55°. Actually, the experimental CEP is only measured up to an unknown offset. In the experiment, Bergues *et al.* [11] used the theoretical Ar^+ asymmetry as a reference to set the value of the offset such that the maximum of the measured Ar^+ asymmetry curve coincided with the maximum of the calculated one. With the absolute values of the CEP determined in this way, the phase of the asymmetry for Ar^{2+} calculated by using the 1D semiclassical model, however, exhibits a discrepancy of 40° with respect to the measured one [11]. This discrepancy of about 40° seems to persist when varying the intensity [43]. In addition, as shown in Fig. 7, with a 3D classical ensemble model the phase of the calculated Ar^+ asymmetry of Huang *et al.* [13] is also different from experiment by about 35°.

It should be noted that the simulated results of Huang *et al.* [13] consist of the contributions from both RESI and RDI. It was claimed that the two mechanisms of RDI and RESI make comparable contributions to NSDI for all CEPs [13]. Generally, in classical simulations, the two main double-ionization energy-transfer pathways are identified by using the time difference t_{diff} between the recollision time and the double ionization time. Although t_{diff} is a positive but arbitrary parameter, it has now been widely accepted that the NSDI events with a time difference less than about $0.1T$, where T is the optical period, are counted as RDI [13,15,42,44]. By choosing $t_{\text{diff}} = 0.1T$, the 3D classical simulations of Chen *et al.* [15] also revealed that, for the laser parameters used in [11], the number of RDI events is about three times larger than that of

Optics EXPRESS

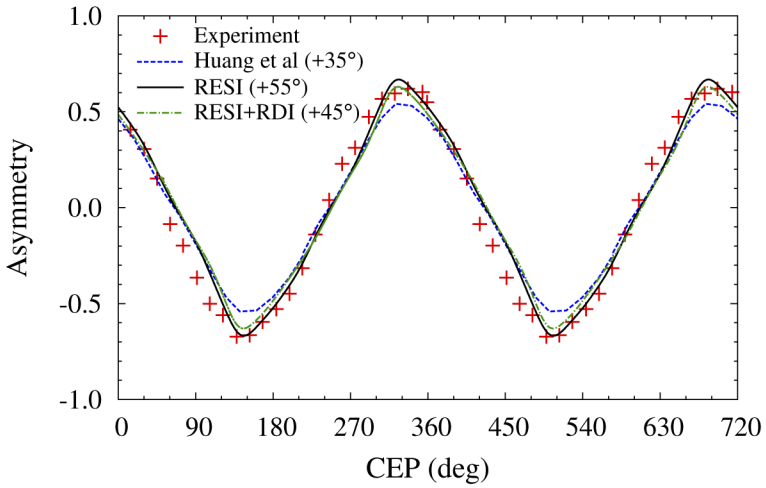

Fig. 7. Comparison of the experimental and calculated asymmetries as a function of the CEP for Ar^{2+}. The experimental data (crosses) are taken from Bergues *et al.* [11]. The calculated results of 3D classical ensemble model (broken curve) by Huang *et al.* [13] are shifted by 35°, and the simulated results of present QRS model are shifted by 55° and 45° for RESI (solid curve) and RESI+RDI (chain curve), respectively.

RESI, which is even larger than that predicted by Huang *et al.* [13]. However, a basic analysis of the calculated TCSs for electron impact ionization and electron impact excitation of Ar^+, as shown in Fig. 1(d), clearly indicates that, under the conditions of the experiment performed by Bergues *et al.* [11], in which the maximum energy of the returning electron is about 50 eV, RSDI constitutes the main contribution to NSDI of Ar. The fact that the classical simulations always predicted a larger number of RDI events for the cases considered here may indicate that this classification method, while valid for long pulses, is no longer applicable for near-single-cycle laser pulses. For long pulses, recollision often takes place at the time when electric field is close to zero, whereas for short pulses the returning electron possesses more chances to recollide with the parent ion at the instant near the peak of electric field, as demonstrated in Fig. 5 of [13]. Consequently, tunneling ionization could take a much shorter time, thereby leading to RESI with $t_{\rm diff}<0.1T$. As a result, the number of RDI events could have easily been overestimated in the classical simulations [13,15].

We also performed calculations for the CMD of RDI. The Ar^{2+} asymmetry obtained from the entire CMD for NSDI as a function of the CEP is plotted in Fig. 7. With the contribution of RDI included, the Ar^{2+} asymmetry shrinks a little with respect to that of RESI and exhibits a discrepancy of 45° compared to experiment.

3.2.2. Correlated momentum distributions

In Fig. 8 we show a direct comparison of the simulated CMD with the corresponding experimental measurements. Due to the discrepancy of 55° in the phase of the Ar^{2+} asymmetry between theory and experiment, we choose the simulated CMD for $\phi = 275°$ to compare with the experimental data for $\phi = 330°$. By comparing Figs. 8(a) and 8(d) with Figs. 8(c) and 8(f), respectively, for both the selected CEP and the CEP-averaged CMD, the QRS model reproduces well the overall pattern of the experimental findings, even though the RDI process has not been taken into account. The main difference is that the computed CMD have more double ionization events with both electron momenta being close to zero. To identify the contribution of RDI, we display the CMD for the entire NSDI including both RESI and RDI in Figs. 8(b) and 8(e), respectively.

Optics EXPRESS

Our results clearly demonstrate that, for the situations considered here, the contribution of RDI is not significant compared to that of RESI. This is in striking contrast to the conclusions drawn in [13,15]. In addition, while it was argued in [13] that RDI events contribute to the inner part of the cross-shaped structure whereas RESI events are responsible for the outer part of the cross-shaped structure, our simulations show that the RDI events are distributed in the first and third quadrants far away from the center. These remarkable differences between the QRS model and the classical model might indicate that in the classical simulations, (i) using the time interval between the final double ionization and the recollision to define the RDI and RESI is sometimes unreasonable, especially for the case of short pulses, and (ii) the selected sample trajectories do not necessarily represent the general situation in which NSDI takes place.

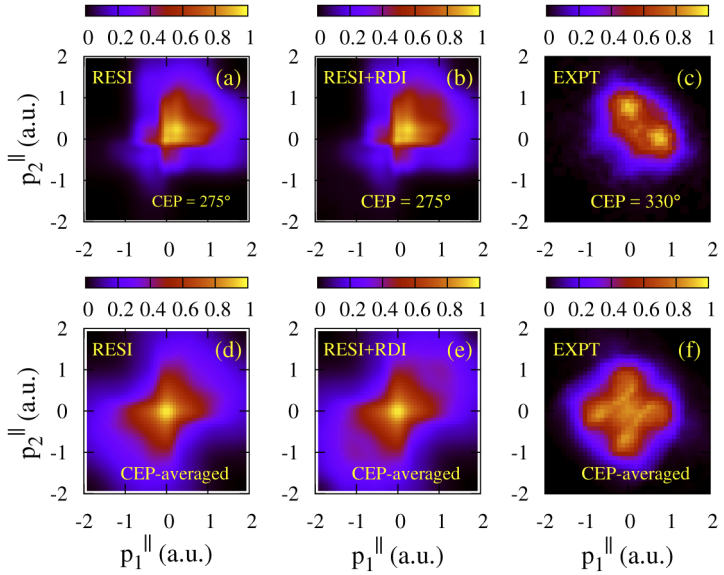

Fig. 8. Comparison of the calculated correlated two-electron parallel momentum distributions with the experimental measurements. See text for details.

It should be noted that apart from RESI and RDI, NSDI could also take place through sequential ionization of doubly excited states (SIDE) which are populated after the laser-induced recollision [42,44,45]. Unfortunately, the present QRS model is still unable to predict the momentum distributions for SIDE, although the mechanism can be interpreted qualitatively. However, a recent theoretical study based on a semiclassical model showed that, while SIDE dominates NSDI of Ar when the laser intensities are below the recollision threshold, the contribution of SIDE to NSDI decreases rapidly as the intensity increases, and the ratio of SIDE/NSDI becomes about 7% for the laser intensity considered here [42].

Interestingly, one can see that the CEP-averaged experimental CMD in Fig. 8(f) exhibits two lines parallel to the main diagonal. This feature is entirely absent in the present simulated momentum distributions and the existing classical simulations as well. We note that a similar, even more pronounced "double-line" structure also exists in the measured CMD for NSDI of helium in [6], where this "double-line" was attributed to the H_2^+ background from cold H_2 in the gas jet.

Finally, as also demonstrated in [15,22], for the relatively low laser intensity considered here, the focal-volume effect could be safely neglected. At high intensities, on the other hand, inclusion of the focal-volume effect might dramatically change the pattern of the simulated

Optics EXPRESS

CMDs compared to those obtained without focal-volume averaging. In the present simulations, therefore, the integral over the focal volume has not been performed.

4. Summary and conclusions

With differential cross sections for electron impact excitation of Ar^+ calculated with the state-of-the-art multi-electron *B*-spline *R*-matrix close-coupling theory, we simulated the correlated two-electron momentum distributions (CMD) for NSDI of Ar by near-single-cycle 750 nm laser pulses at an intensity of 2.8×10^{14} W/cm^2 for CEPs ranging from 5° to 155° in steps of 30°, based on the improved quantitative rescattering (QRS) model. The overall pattern of both the CEP-resolved and CEP-averaged CMDs measured in experiment are well reproduced by the QRS model. In addition, by shifting the phase by about 45°, the simulated asymmetries for the doubly charged ion are in excellent agreement with experiment. Our results demonstrate that under the experimental conditions considered here, the contributions of RDI can be safely neglected. This contradicts the arguments made in [13,15] based on 3D classical and semiclassical simulations. Our findings suggest that classical trajectory analysis might not be applicable for short pulses. Our investigations also reveal that the cross-shaped structure is attributed to the strong forward scattering of the returning electron, as well as the depletion effect in tunneling ionization. This is in accord with the conclusions drawn by Bergues *et al.* [11] using a 1D semiclassical model. However, it should be noted that, with the selected scattering angle and the selected lowest excited state, the 1D semiclassical results cannot validate the assumptions of the model, since the choice of the lower-lying excited states and their relative contributions remain ambiguous without knowledge of the electron impact excitation cross sections. The present theoretical study based on fully quantum-mechanical calculations should settle the existing controversial debate on the mechanisms responsible for the cross-shaped structure observed experimentally.

Funding

National Science Foundation (OAC-1834740, PHY-090031, PHY-1803844); Japan Society for the Promotion of Science (19H00887); Guangdong Province Introduction of Innovative R&D Team (2018KTSCX062); Science and Technology Planning Project of Guangdong Province (180917124960522); National Natural Science Foundation of China (11274219).

Acknowledgments

ZC wishes to thank Dr. M. F. Kling for providing the experimental data plotted in Fig. 8 in digital form.

Disclosures

The authors declare no conflicts of interest.

References

1. W. Becker, X. J. Liu, P. J. Ho, and J. H. Eberly, "Theories of photoelectron correlation in laser-driven multiple atomic ionization," Rev. Mod. Phys. **84**(3), 1011–1043 (2012).
2. A. L'Huillier, L. A. Lompre, G. Mainfray, and C. Manus, "Multiply charged ions formed by multiphoton absorption processes in the continuum," Phys. Rev. Lett. **48**(26), 1814–1817 (1982).
3. B. Walker, B. Sheehy, L. F. DiMauro, P. Agostini, K. J. Schafer, and K. C. Kulander, "Precision measurement of strong field double ionization of helium," Phys. Rev. Lett. **73**(9), 1227–1230 (1994).
4. T. Weber, H. Giessen, M. Weckenbrock, G. Urbasch, A. Staudte, L. Spielberger, O. Jagutzki, V. Mergel, M. Vollmer, and R. Dörner, "Correlated electron emission in multiphoton double ionization," Nature **405**(6787), 658–661 (2000).
5. B. Feuerstein, R. Moshammer, D. Fischer, A. Dorn, C. D. Schröter, J. Deipenwisch, J. R. C. Lopez-Urrutia, C. Höhr, P. Neumayer, J. Ullrich, H. Rottke, C. Trump, M. Wittmann, G. Korn, and W. Sandner, "Separation of recollision mechanisms in nonsequential strong field double ionization of Ar: The role of excitation tunneling," Phys. Rev. Lett. **87**(4), 043003 (2001).

Optics EXPRESS

6. A. Staudte, C. Ruiz, M. Schöffler, S. Schössler, D. Zeidler, T. Weber, M. Meckel, D. M. Villeneuve, P. B. Corkum, A. Becker, and R. Dörner, "Binary and recoil collisions in strong field double ionization of helium," Phys. Rev. Lett. **99**(26), 263002 (2007).
7. A. Rudenko, V. L. B. de Jesus, T. Ergler, K. Zrost, B. Feuerstein, C. D. Schröter, R. Moshammer, and J. Ullrich, "Correlated two-electron momentum spectra for strong-field nonsequential double ionization of He at 800 nm," Phys. Rev. Lett. **99**(26), 263003 (2007).
8. Y. Liu, D. Ye, J. Liu, A. Rudenko, S. Tschuch, M. Dürr, M. Siegel, U. Morgner, Q. Gong, R. Moshammer, and J. Ullrich, "Multiphoton Double Ionization of Ar and Ne Close to Threshold," Phys. Rev. Lett. **104**(17), 173002 (2010).
9. J. Krause, K. Schafer, and K. Kulander, "High-order harmonic generation from atoms and ions in the high intensity regime," Phys. Rev. Lett. **68**(24), 3535–3538 (1992).
10. P. B. Corkum, "Plasma perspective on strong field multiphoton ionization," Phys. Rev. Lett. **71**(13), 1994–1997 (1993).
11. B. Bergues, M. Kübel, N. G. Johnson, B. Fischer, N. Camus, K. J. Betsch, O. Herrwerth, A. Senftleben, A. M. Sayler, T. Rathje, T. Pfeifer, I. Ben-Itzhak, R. R. Jones, G. G. Paulus, F. Krausz, R. Moshammer, J. Ullrich, and M. F. Kling, "Attosecond tracing of correlated electron-emission in non-sequential double ionization," Nat. Commun. **3**(1), 813 (2012).
12. C. F. de Morisson Faria, T. Shaaran, and M. T. Nygren, "Time-delayed nonsequential double ionization with few-cycle laser pulses: Importance of the carrier-envelope phase," Phys. Rev. A **86**(5), 053405 (2012).
13. C. Huang, Y. Zhou, Q. Zhang, and P. Lu, "Contribution of recollision ionization to the cross-shaped structure in nonsequential double ionization," Opt. Express **21**(9), 11382–11390 (2013).
14. M. Kübel, C. Burger, N. G. Kling, T. Pischke, L. Beaufore, I. Ben-Itzhak, G. G. Paulus, J. Ullrich, T. Pfeifer, R. Moshammer, M. F. Kling, and B. Bergues, "Complete characterization of single-cycle double ionization of argon from the nonsequential to the sequential ionization regime," Phys. Rev. A **93**(5), 053422 (2016).
15. A. Chen, M. Kübe, B. Bergues, M. F. Kling, and A. Emmanouilidou, "Non-sequential double ionization with near-single cycle laser pulses," Sci. Rep. **7**(1), 7488 (2017).
16. M. Kübel, N. G. Kling, K. J. Betsch, N. Camus, A. Kaldun, U. Kleineberg, I. Ben-Itzhak, R. R. Jones, G. G. Paulus, T. Pfeifer, J. Ullrich, R. Moshammer, M. F. Kling, and B. Bergues, "Nonsequential double ionization of N2 in a near-single-cycle laser pulse," Phys. Rev. A **88**(2), 023418 (2013).
17. Z. Chen, Y. Liang, and C. D. Lin, "Quantum theory of recollisional (e, $2e$) process in strong field nonsequential double ionization of helium," Phys. Rev. Lett. **104**(25), 253201 (2010).
18. Z. Chen, Y. Liang, and C. D. Lin, "Quantitative rescattering theory of correlated two-electron momentum spectra for strong-field nonsequential double ionization of helium," Phys. Rev. A **82**(6), 063417 (2010).
19. Z. Chen, Y. Zheng, W. Yang, X Song, J. Xu, L. F. DiMauro, O. Zatsarinny, K. Bartschat, T. Morishita, S.-F. Zhao, and C. D. Lin, "Numerical simulation of the double-to-single ionization ratio for the helium atom in strong laser fields," Phys. Rev. A **92**(6), 063427 (2015).
20. Z. Chen, Y. Wang, L. Zhang, and X. Jia, "Revisiting the recollisional (e, $2e$) process in strong-field nonsequential double ionization of helium," Phys. Rev. A **99**(3), 033401 (2019).
21. Z. Chen, Y. Wang, T. Morishita, X. Hao, J. Chen, O. Zatsarinny, and K. Bartschat, "Revisiting the recollisional excitation-tunneling process in strong-field nonsequential double ionization of helium," Phys. Rev. A **100**(2), 023405 (2019).
22. Z. Chen, H. Wen, F. Liu, T. Morishita, O. Zatsarinny, and K. Bartschat, "Intensity dependence in nonsequential double ionization of helium," Opt. Express **28**(5), 6490–6504 (2020).
23. T. Morishita, A.-T. Le, Z. Chen, and C. D. Lin, "Accurate retrieval of structural information from laser-induced photoelectron and high-order harmonic spectra by few-cycle laser pulses," Phys. Rev. Lett. **100**(1), 013903 (2008).
24. T. Morishita and O. I. Tolstikhin, "Adiabatic theory of strong-field photoelectron momentum distributions near a backward rescattering caustic," Phys. Rev. A **96**(5), 053416 (2017).
25. Y. Okajima, O. I. Tolstikhin, and T. Morishita, "Adiabatic theory of high-order harmonic generation: One-dimensional zero-range-potential model," Phys. Rev. A **85**(6), 063406 (2012).
26. O. I. Tolstikhin and T. Morishita, "Strong-field ionization, rescattering, and target structure imaging with vortex electrons," Phys. Rev. A **99**(6), 063415 (2019).
27. Z. Chen, A.-T. Le, T. Morishita, and C. D. Lin, "Quantitative rescattering theory for laser-induced high-energy plateau photoelectron spectra," Phys. Rev. A **79**(3), 033409 (2009).
28. A.-T. Le, R. R. Lucchese, S. Tonzani, T. Morishita, and C. D. Lin, "Quantitative rescattering theory for high-order harmonic generation from molecules," Phys. Rev. A **80**(1), 013401 (2009).
29. Z. Chen, Y. Liang, D. H. Madison, and C. D. Lin, "Strong-field nonsequential double ionization of Ar and Ne," Phys. Rev. A **84**(2), 023414 (2011).
30. O. Zatsarinny, "BSR: B-spline atomic R-matrix codes," Comput. Phys. Commun. **174**(4), 273–356 (2006).
31. O. Zatsarinny and K. Bartschat, "The B-spline R-matrix method for atomic processes: application to atomic structure, electron collisions and photoionization," J. Phys. B: At. Mol. Phys. **46**(11), 112001 (2013).
32. T. Morishita, Z. Chen, S. Watanabe, and C. D. Lin, "Two-dimensional electron momentum spectra of argon ionized by short intense lasers: Comparison of theory with experiment," Phys. Rev. A **75**(2), 023407 (2007).
33. H. W. van der Hart and K. Burnett, "Recollision model for double ionization of atoms in strong laser fields," Phys. Rev. A **62**(1), 013407 (2000).

Optics EXPRESS

34. E. Eremina, X. Liu, H. Rottke, W. Sandner, A. Dreischuh, F. Lindner, F. Grasbon, G. G. Paulus, H. Walther, R. Moshammer, B. Feuerstein, and J. Ullrich, "Laser-induced non-sequential double ionization investigated at and below the threshold for electron impact ionization," J. Phys. B: At. Mol. Phys. **36**(15), 3269–3280 (2003).
35. Z. Chen, D. H. Madison, C. T. Whelan, and H. R. J. Walters, "Second-order distorted wave calculation for electron impact ionization of hydrogen," J. Phys. B: At. Mol. Phys. **37**(5), 981–995 (2004).
36. Z. Chen and D. H. Madison, "Second-order distorted wave calculation for electron-impact ionization of helium to He^+ ($n = 1$ and 2)," J. Phys. B: At. Mol. Phys. **38**(23), 4195–4209 (2005).
37. Z. Chen, F. Liu, and H. Wen, "Quantitative rescattering theory for nonsequential double ionization," Chin. Phys. B **28**(12), 123401 (2019).
38. W. Lotz, "Electron-impact ionization cross sections and ionization rate coefficents for atoms and ions from hydrogen to calcium," Eur. Phys. J. A **216**(3), 241–247 (1968).
39. A. Müller, K. Hubert, K. Tinschert, R Becker, and E. Salzborn, "An improved crossed-beams technique for the measurement of absolute cross sections for electron impact ionisation of ions and its application to Ar^+ ions," J. Phys. B: At. Mol. Phys. **18**(14), 2993–3009 (1985).
40. M. V. Ammosov, N. B. Delone, and V. P. Krainov, "Tunnel ionization of complex atoms and of atomic ions in an alternating electromagnetic field," Sov. Phys. JETP **64**, 1191–1194 (1986).
41. X. M. Tong and C. D. Lin, "Empirical formula for static field ionization rates of atoms and molecules by lasers in the barrier-suppression regime," J. Phys. B: At. Mol. Phys. **38**(15), 2593–2600 (2005).
42. Z. Chen, X. Li, X. Sun, X. Hao, and J. Chen, "Identification of doubly excited states in nonsequential double ionization of Ar in strong laser fields," J. Phys. B: At. Mol. Phys. **50**(24), 245601 (2017).
43. M. Kübel, "Single-cycle non-sequential double ionization," Dept. Physics, Ludwig-Maximilians Univ., Munich, Germany, (2014).
44. Z. Zhang, L. Bai, and J. Zhang, "Double ionization of Ar below the recollision threshold intensity," Phys. Rev. A **90**(2), 023410 (2014).
45. Y. Liu, L. Fu, D. Ye, J. Liu, M. Li, C. Wu, Q. Gong, R. Moshammer, and J. Ullrich, "Strong-Field Double Ionization through Sequential Release from Double Excitation with Subsequent Coulomb Scattering," Phys. Rev. Lett. **112**(1), 013003 (2014).

132.234.229.188 {ts '2020-10-27 22:25:44'}